Nano Research 2015, 8(8): 2663–2675
DOI 10.1007/s12274-015-0773-3
Research Article
ISSN 1998-0124
CN 11-5974/O4

Hollow-in-hollow carbon spheres with hollow foam-like cores for lithium–sulfur batteries

Jun Zang[1,2], Taihua An[2], Yajie Dong[1], Xiaoliang Fang[1] (✉), Mingsen Zheng[2], Quanfeng Dong[2], and Nanfeng Zheng[2] (✉)

[1] *Pen-Tung Sah Institute of Micro-Nano Science and Technology, Xiamen University, Xiamen 361005, China*
[2] *State Key Laboratory for Physical Chemistry of Solid Surfaces, Collaborative Innovation Center of Chemistry for Energy Materials, and Department of Chemistry, College of Chemistry and Chemical Engineering, Xiamen University, Xiamen 361005, China*

Received: 2 February 2015
Revised: 22 March 2015
Accepted: 24 March 2015

KEYWORDS
hollow spheres,
porous carbon,
sulfur/carbon cathode,
lithium–sulfur batteries

ABSTRACT

Lithium–sulfur batteries have attracted increasing attention because of their high theoretical capacity. Using sulfur/carbon composites as the cathode materials has been demonstrated as an effective strategy to optimize sulfur utilization and enhance cycle stability as well. In this work, hollow-in-hollow carbon spheres with hollow foam-like cores (HCSF@C) are prepared to improve both capability and cycling stability of lithium–sulfur batteries. With high surface area and large pore volumes, the loading of sulfur in HCSF@C reaches up to 70 wt.%. In the resulting S/HCSF@C composites, the outer carbon shell serves as an effective protection layer to trap the soluble polysulfide intermediates derived from the inner component. Consequently, the S/HCSF@C cathode retains a high capacity of 780 mAh/g after 300 cycles at a high charge/discharge rate of 1 A/g.

1 Introduction

Lithium–sulfur batteries, one of the most promising next-generation high-energy storage systems, have attracted increasing attention due to their high theoretical specific energy of 2,600 Wh/kg [1–5]. Based on the electrochemical reaction of $16Li + S_8 \rightarrow 8Li_2S$, a sulfur cathode can provide a high theoretical capacity of 1,675 mAh/g, which is 3 to 5 times higher than those of lithium-ion batteries based on conventional insertion compound cathodes [4]. In addition to high theoretical capacity, using sulfur as the active cathode material brings the advantages of its high natural abundance, nontoxicity, low cost, and environmental friendliness. Despite their advantages, lithium–sulfur batteries still suffer from several inherent drawbacks [1–5]. Firstly, the poor electronic conductivity of sulfur and its discharge products (Li_2S/ Li_2S_2) leads to the low utilization of active materials. Secondly, polysulfide intermediates (Li_2S_x, $4 \leqslant x \leqslant 8$) formed during the charge/discharge processes are soluble in the electrolyte and can shuttle between anode and cathode

Address correspondence to Nanfeng Zheng, nfzheng@xmu.edu.cn; Xiaoliang Fang, x.l.fang@xmu.edu.cn

during cycling (i.e., there is a "shuttle effect"), resulting in loss of active materials and poor cycle life. Finally, the large volumetric expansion/shrinkage of sulfur during lithiation/delithiation gradually decreases the mechanical integrality and stability of cathode [6].

To address the above issues, various sulfur-based composites have been proposed to modulate the sulfur cathodes, such as sulfur/carbon composites [7–9], sulfur/conductive polymer composites [10], polymer or graphene coated sulfur/carbon composites [11–13], and sulfur nanoparticles encapsulated inside hollow TiO_2 shells or hollow conductive polymer shells [14, 15]. Other strategies include placing an interlayer between the sulfur cathode and separator [16], and employing $LiNO_3$ as an electrolyte additive to protect the anode [17]. The fabrication of sulfur/carbon composites with high sulfur utilization, capacity, and cycle stability is considered as one of the most promising strategies. Since the porous carbon matrix can significantly confine polysulfides and reduce the "shuttle effect" [7], a variety of porous carbon materials, such as ordered mesoporous/ microporous carbon [18–20], porous carbon spheres [21, 22], porous carbon tubes [23, 24], layered porous carbon [8, 25, 26], hierarchical porous carbon [27–30], and microporous carbon fibers [31, 32], have been adopted as host substrates for sulfur cathodes. Among the available porous carbon nanostructures, hollow carbon spheres (HCS) with high specific surface area and large pore volumes that can allow for higher sulfur content and the effective suppression of polysulfide dissolution provided new opportunities and has been successfully used in sulfur/carbon cathodes [33–37]. Although the porous structure with high pore volumes favors high sulfur loading, the gradual capacity decay upon cycling is reduced only by the weak interactions between sulfur and the porous carbon shell. Therefore, it is still a challenge to design HCS that combines high sulfur loading with less "shuttle effect" to achieve high-performance sulfur/carbon cathodes [38].

As a special class of hollow structures, hollow nanospheres decorated with functionalized cores, which are called "rattle" or "yolk–shell" structures, have been considered an effective way to improve the performance of hollow nanospheres [39, 40]. Very recently, hollow-in-hollow oxide materials with hollow cores have been successfully developed to fabricate high-performance lithium ion battery anodes [41, 42]. The hollow-in-hollow structure has been demonstrated to improve the capacity and charge retention of hollow metal oxide spheres due to the better utilization of the void interior [41, 42]. From the viewpoint of fundamental research, the synthesis of hollow-in-hollow carbon spheres with hollow cores (designated as HCS@C) based on the corresponding HCS offers a way to investigate and understand the advantages of hollow-in-hollow structure. Compared with HCS, HCS@C is expected to have higher volume density and shorter diffusion lengths for Li^+ ions and electrons, making them promising candidates for the high performance sulfur/carbon cathodes. More importantly, the "shuttle effect" should be well-suppressed by the structural design of the porous carbon host which is highly desirable for the high-performance sulfur/carbon cathodes [36].

Herein, we report a facile hard-templating method for the synthesis of hollow carbon spheres with foam-like shells (HCSF), and hollow-in-hollow carbon spheres with hollow foam-like cores (HCSF@C). With high specific surface area and large pore volumes, the as-synthesized HCSF and HCSF@C were employed in the fabrication of sulfur/carbon cathodes. The electrochemical properties of the as-synthesized S/HCSF cathode and S/HCSF@C cathode demonstrate that the dissolution/diffusion of polysulfide can be greatly reduced by the hollow-in-hollow structure. The outer carbon shell of S/HCSF@C can act as a protective layer to alleviate the loss of soluble active polysulfide species derived from the inner hollow foam-like S/HCSF cores. By understanding the role of the hollow carbon shell in S/HCSF@C, we optimized the structure parameters of S/HCSF@C to maximize the sulfur loading. The active mass of the optimized S/HCSF@C can be as high as 70.7 wt.% sulfur, which is desirable for practical applications. Compared with the S/HCSF cathode, the optimized S/HCSF@C cathode exhibits higher specific capacity, and significantly enhanced cycling stability and rate capability.

2 Experimental

2.1 Materials

Tetraethyl orthosilicate (TEOS) and resorcinol (R), were purchased from Alfa Aesar; ammonia solution (25%–28%), cetyltrimethyl ammonium bromide (CTAB), ethanol, sublimed sulfur, and formaldehyde (F) were purchased from Sinopharm Chemical Reagent Co. (Shanghai, China). All the reagents were used without further purification. Deionized water was used in all experiments.

2.2 Synthesis of SiO_2 spheres

SiO_2 spheres were obtained via a slightly modified Stöber process. In a typical synthesis, 6 mL of TEOS was rapidly added into a mixture of 75 mL of ethanol, 10 mL of deionized water, and 3.15 mL of aqueous ammonia solution, and the mixture stirred at room temperature for 1 h. The as-synthesized SiO_2 spheres were centrifugally separated from the suspension and washed with deionized water and ethanol.

2.3 Synthesis of HCSF, HCSF@C, S/HCSF and S/HCSF@C

1 g of the as-synthesized SiO_2 spheres was homogeneously dispersed in 10 mL of deionized water by ultrasonication for 15 min. The suspension was then added into a solution containing CTAB (0.75 g), deionized water (110 mL) and ethanol (48 mL). After the mixture was stirred at room temperature for 0.5 h, 0.32 g of R, 0.45 mL of F and 2 mL of aqueous ammonia solution were added in sequence. The final mixture was stirred at 30 ℃ for 16 h, and the resulting SiO_2@RF spheres (i.e., RF resin coated SiO_2 spheres) were collected by centrifugation and washed with ethanol. The as-prepared SiO_2@RF spheres were homogeneously dispersed in a mixture of 75 mL of ethanol, 10 mL of deionized water, and 3.15 mL of aqueous ammonia solution by ultrasonication. Then 1 mL of TEOS was added with vigorous stirring every 1 h up to a total TEOS volume of 3 mL. The resultants SiO_2@RF@SiO_2 spheres were collected by centrifugation and washed with deionized water. The SiO_2@RF@SiO_2@RF@SiO_2 spheres were obtained by treating SiO_2@RF@SiO_2 spheres with the same silica coating and RF coating procedures. The intermediates SiO_2@C@SiO_2 spheres and SiO_2@C@SiO_2@C@SiO_2 spheres were obtained by the carbonization of the as-synthesized SiO_2@RF@SiO_2 spheres and SiO_2@RF@SiO_2@RF@SiO_2 spheres under N_2 atmosphere at 350 ℃ for 2 h with a heating rate of 1.5 ℃/min, which were followed by further treatment at 800 ℃ for 4 h with a heating rate of 1.5 ℃/min. After washing in 10% HF aqueous solution for 24 h, the intermediates SiO_2@C@SiO_2 spheres and SiO_2@C@SiO_2@C@SiO_2 spheres were converted into hollow HCSF and hollow-in-hollow structured HCSF@C, respectively.

The sulfur/carbon composites were prepared by the melt–diffusion approach. 0.1 g of the as-synthesized HCSF or HCSF@C was mixed with 0.3 g of sublimed sulfur. The mixture was then heated at 155 ℃ for 6 h. After cooling down to room temperature, the sulfur/carbon composites were obtained.

2.4 Characterization

Scanning electron microscopy (SEM) and transmission electron microscopy (TEM) images were taken on a Zeiss SIGMA microscope and a TECNAI F-30 high-resolution transmission electron microscope operating at 300 kV, respectively. The specific surface area of the as-synthesized HCSF, HCSF@C, S/HCSF, and S/HCSF@C were measured by the Brunauer–Emmett–Teller (BET) method using nitrogen adsorption and desorption isotherms on a Micrometrics ASAP 2020 system. Pore size distribution plots were obtained by the Barrett–Joyner–Halenda method. Thermogravimetric analysis (TGA) was performed using a Pyris Diamond TG-DTA (PE Co., USA).

2.5 Electrochemical measurements

The electrochemical performances of the sulfur/carbon composites were evaluated using CR2016 type coin cells. The working electrodes were made up by 70 wt.% sulfur/carbon composites, 20 wt.% super P and 10 wt.% water soluble polymer n-lauryl acrylate (LA Chengdu, China). Al foil was used as the current collector and Li foil was used as the counter electrode. The electrolyte was 0.6 M bis(trifluoromethanesulfonyl)imide lithium in a mixed solvent of 1,2-dimethoxyethane and 1,3-dioxolane (v/v = 1:1) with 0.4 M $LiNO_3$ and the separator was Celgard 2400

polypropylene membrane. Cell assembly was carried out in an Ar-filled glovebox with the concentrations of moisture and oxygen below 1 ppm. The cells were galvanostatically charged and discharged between 1.9 and 3.0 V vs. Li^+/Li using a BTS Battery Tester (Neware, Shenzhen, China) under various current densities (100, 200, 500 mA/g, 1 and 2 A/g).

3 Results and discussion

3.1 Formation and characterization of HCSF, HCSF@C, S/HCSF, and S/HCSF@C

Figure 1(a) illustrates the typical hard-templating procedure for the synthesis of HCSF and HCSF@C. Firstly, the SiO_2 spheres were coated with resorcinol–formaldehyde resin and SiO_2 layers via our recent reported cationic surfactant assisted RF resin coating strategy [43, 44]. After the carbonization under N_2 atmosphere and the subsequent removal of the SiO_2 by HF aqueous solution, the-synthesized SiO_2@RF@SiO_2 spheres were converted into HCSF. HCSF@C with a hollow-in-hollow structure was obtained through the similar procedure but simply replacing the SiO_2 spheres with the-synthesized SiO_2@RF@SiO_2 spheres. When the ratio of inner layer RF precursors and outer layer RF precursors was 1, the as-synthesized HCSF@C is denoted as HCSF@C-1.

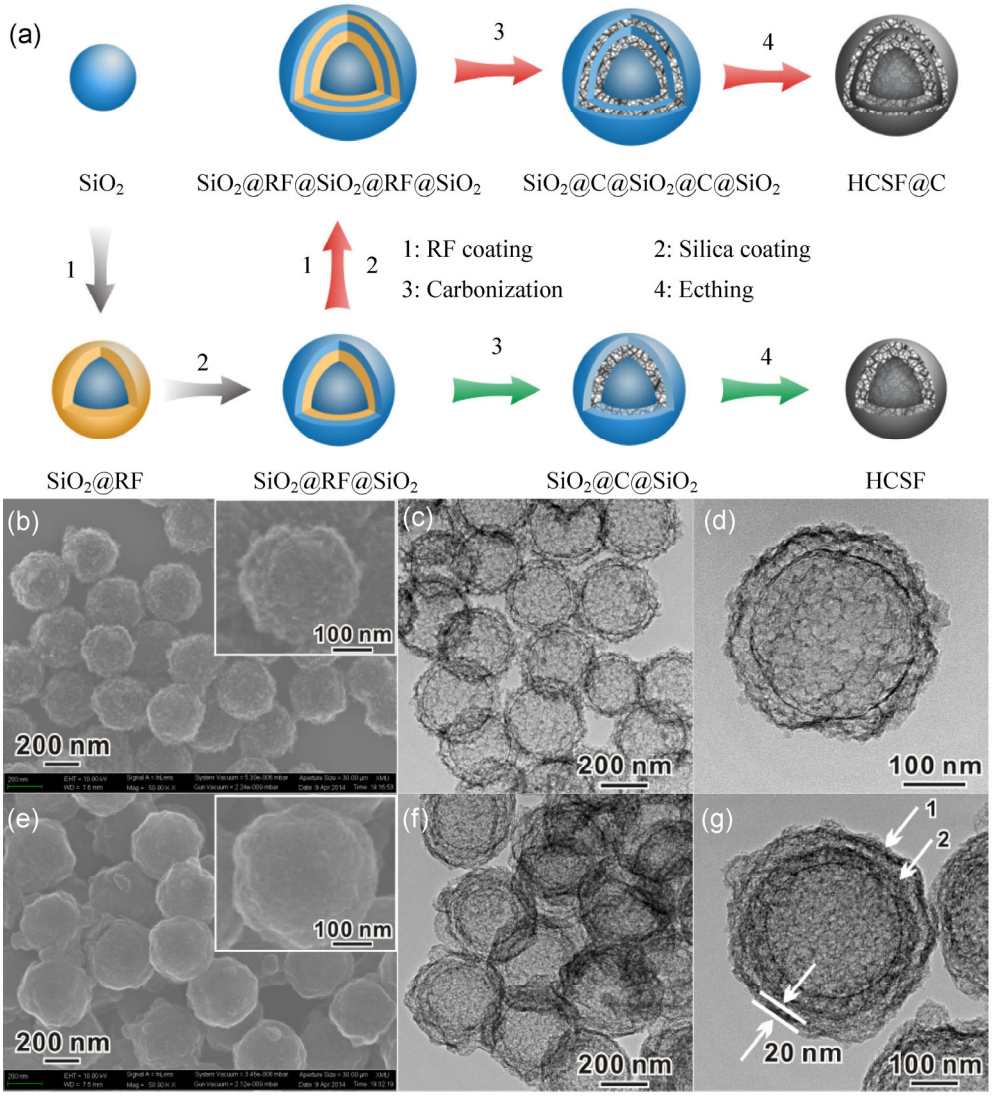

Figure 1 (a) Schematic illustration: the hard-templating procedures for the synthesis of HCSF and HCSF@C, (b) SEM image and (c) and (d) TEM images of HCSF, (e) SEM image and (f) and (g) TEM images of HCSF@C-1.

The structures and morphologies of HCSF and HCSF@C-1 were characterized by SEM and TEM, respectively. Figure 1(b) shows the typical SEM image of spherical HCSF with diameter of ~350 nm (Fig. S1, in the Electronic Supplementary Material (ESM)). The TEM image of HCSF (Fig. 1(c)) reveals that the as-synthesized HCSF possesses a uniform hollow structure, and the interior hollow size of HCSF agrees well with the diameter of the SiO_2 templates. The average thickness of the porous carbon shell in HCSF is about 50 nm. Additionally, the porous carbon shell of HCS displays an obvious foam-like structure, which is similar to the SnO_2 derived double-shelled HCS (DHCS) with carbon "links" connecting the two shells [34]. The high-magnification TEM image of HCSF (Fig. 1(d)) further reveals that the hollow foam-like carbon core of HCSF exhibits a porous network structure with pore sizes in the range of several nanometers to tens of nanometers. In comparison, HCSF@C-1 exhibits a similar morphology to HCSF with enlarged diameter up to ~400 nm (Fig. 1(e) and Fig. S1 (in the ESM)). As shown in Figs. 1(f) and 1(g), HCSF is encapsulated in a hollow porous carbon shell, resulting in the hollow-in-hollow structure of HCSF@C-1. The inner HCSF core, the outer hollow carbon shell, and the void space between core and shell can be clearly distinguished (see the arrows illustrated in Fig. 1(g)). The average thickness of the outer carbon shell in HCSF@C-1 is about 20 nm. Since the diameter of the SiO_2@RF@SiO_2 templates is bigger than the SiO_2 templates, the thickness of the outer carbon shell in HCSF@C-1 is smaller than that of the inner HCSF core. Furthermore, no obvious foam-like structure was observed in the outer carbon shell of HCSF@C-1.

The porosities of HCSF and HCSF@C-1 were investigated by N_2 adsorption–desorption measurements. As illustrated in Fig. 2, the N_2 sorption isotherms with high nitrogen uptake clearly demonstrate the high porosity of HCSF and HCSF@C-1. The N_2 adsorption isotherm of HCSF@C-1 exhibits an analogous shape to that of HCSF, indicating that the pore structure of HCSF@C-1 is similar to that of HCSF. The BET surface area and pore volume of HCSF are 946 m^2/g and 2.09 cm^3/g, respectively. The pore size distribution curve of HCSF exhibits two peaks at about 2 and 30 nm, corresponding to mesopores and the foam-like structure of HCSF, respectively. Compared with HCSF, HCSF@C-1 has a slightly higher surface area (1124 m^2/g) and total pore volume (2.24 cm^3/g), and a bimodal pore size distribution at 2 and 20 nm. The pore structures of HCSF and HCSF@C-1 determined from N_2 adsorption–desorption measurements agree well with the TEM observations. By virtue of their high specific surface areas, pore volumes, and bimodal pore structures, the as-synthesized HCSF and HCSF@C-1 are expected to be promising conducting frameworks for sulfur loading and electrolyte penetration [36].

Sulfur impregnation of HCSF and HCSF@C-1 was carried out by the classical melt–diffusion process [7]. The as-synthesized sulfur/carbon nanocomposites (i.e., S/HCSF and S/HCSF@C-1) were characterized in detail. The specific surface areas and pore volumes

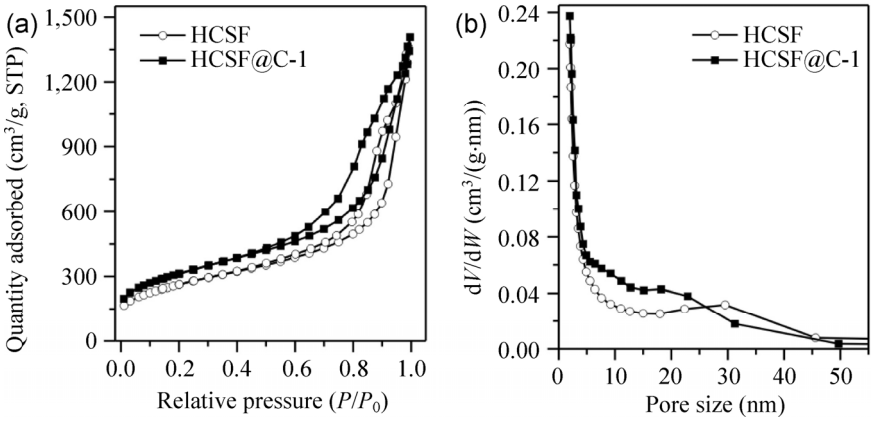

Figure 2 (a) N_2 sorption isotherms and (b) pore size distributions of HCSF and HCSF@C-1.

calculated from the N_2 adsorption–desorption measurements gave direct evidence of the encapsulation of sulfur inside HCSF and HCSF@C-1. After sulfur impregnation, the BET surface area and pore volume of S/HCSF decreased to 13.8 m^2/g and 0.07 m^3/g, respectively. The results for S/HCSF@C-1 also show that the BET surface area (19.1 m^2/g) and pore volume (0.08 m^3/g) decreased after sulfur loading. The X-ray diffraction patterns of the as-synthesized sulfur/carbon nanocomposites contain no obvious characteristic peaks of sulfur, demonstrating that the sulfur exists in a highly dispersed amorphous state (Fig. S2, in the ESM) [29]. As shown in Figs. 3(a) and 3(b), the as-synthesized S/HCSF and S/HCSF@C-1 still retained their original morphologies with no aggregated sulfur particles, indicating that sulfur was fully diffused into the pore structures of HCSF and HCSF@C-1. Meanwhile, energy-dispersive X-ray (EDX) spectra of S/HCSF and S/HCSF@C-1 also indicate the presence of sulfur throughout S/HCSF and S/HCSF@C-1 (Figs. 3(a) and 3(b)). TGA measurements were performed from 30–500 ℃ at a heating rate of 10 ℃/min in N_2 to determine the weight content of sulfur. As shown in Fig. 3(c), S/HCSF shows a weight loss of approximately 71.5% between 200 and 340 ℃, which corresponds to the evaporation of sulfur in the sulfur/carbon nanocomposite [34]. Therefore, the sulfur content in S/HCSF was determined to be approximately 71.5 wt.%. In comparison, the TGA curve of S/HCSF@C-1 indicates that the sulfur content of S/HCSF@C-1 is approximately 70.3 wt.% (Fig. 3(d)). In order to enhance the performance of sulfur cathodes, many sulfur/carbon composites have been reported in the literature, but generally have relatively low sulfur loadings of up to 50 wt.%–60 wt.% [23, 31, 35]. As a carbon host for sulfur loading, the high specific surface areas and pore volumes of the HCS materials obtained in this work can accommodate high loadings of sulfur which should improve the energy density of lithium–sulfur batteries. More importantly, compared with S/HCSF, the sulfur component in S/HCSF@C-1 evaporates over a slightly

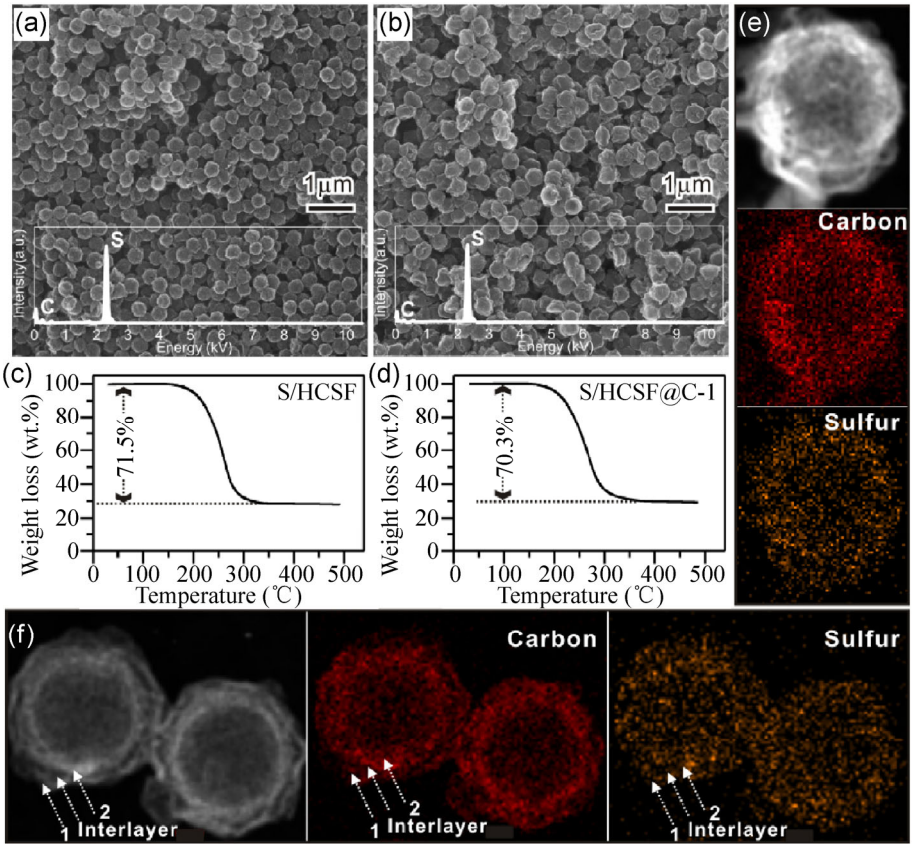

Figure 3 SEM images of (a) S/HCSF and (b) S/HCSF@C-1, TGA curves of (c) S/HCSF and (d) S/HCSF@C-1, element mapping images of (e) S/HCSF and (f) S/HCSF@C-1, inset: EDX spectra of S/HCSF and S/HCSF@C-1.

wider temperature range (200–380 °C), indicating that the sulfur loaded in S/HCSF@C-1 is more stable than that in S/HCSF [34]. To further investigate the sulfur distribution within the as-synthesized sulfur/carbon composites, the element mappings of carbon and sulfur were measured as shown in Figs. 3(e) and 3(f). These demonstrate that sulfur was homogeneously distributed within HCS and HCSF@C-1. Recently, carbon nanotube@hollow porous carbon (CNT@HCP) with a tube-in-tube structure was proposed as a promising carbon host for sulfur/carbon cathodes [45]. After sulfur impregnation, most of sulfur was only incorporated in the outer layer (i.e., the HCP layer) of CNT@HCP. In contrast to CNT@HCP, the mapping of S/HCSF@C-1 showed that the inner HCSF core and the hollow carbon shell of S/HCSF@C-1 were all homogeneously filled with sulfur. No extra sulfur was observed in the carbon interlayer voids or hollow carbon cavities.

3.2 Performance of the as-synthesized S/HCSF and S/HCSF@C in lithium–sulfur batteries

In order to demonstrate the structural benefits of the proposed HCSF@C for improving the performance of sulfur/carbon cathode, a series of electrochemical measurements were carried out. The galvanostatic charge/discharge behavior of the as-synthesized sulfur/carbon cathodes at a charge/discharge rate of 100 mA/g was evaluated within the voltage window of 1.9–3.0 V versus Li^+/Li. As shown in Figs. 4(a) and 4(b),

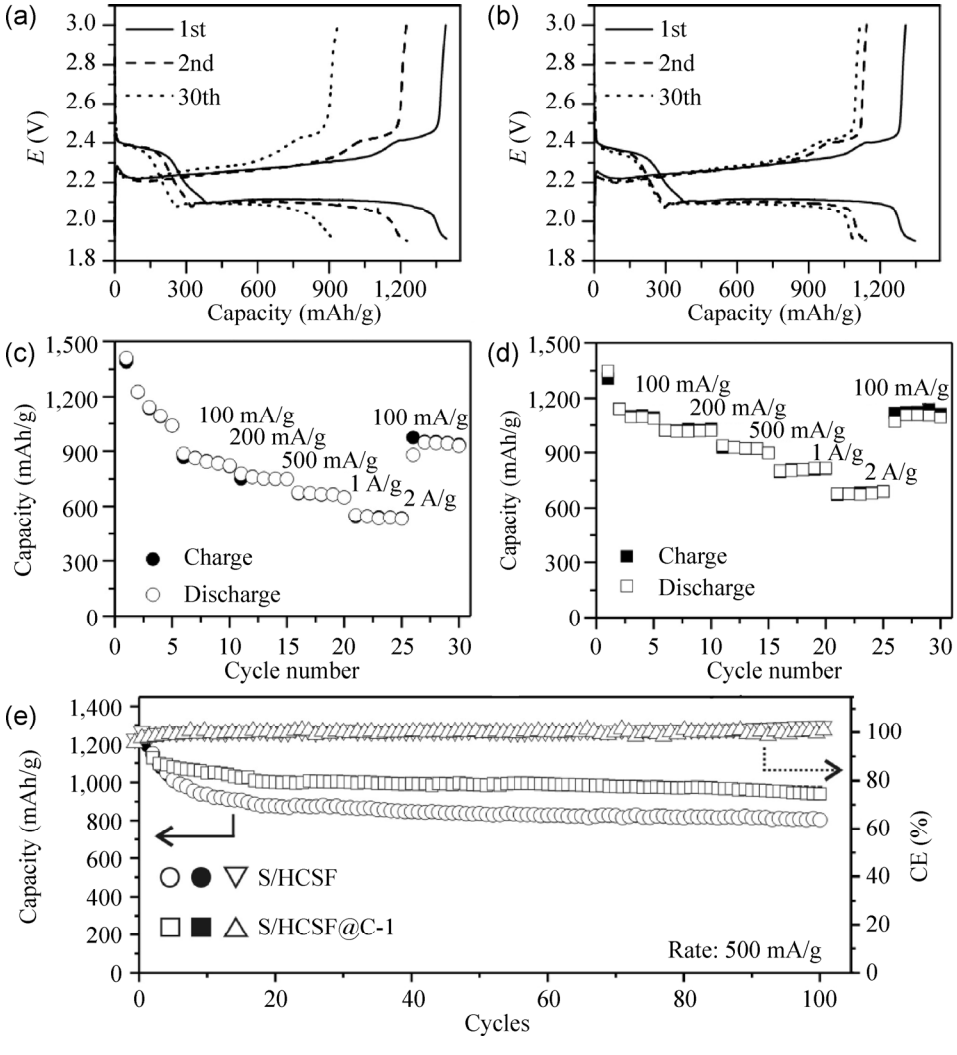

Figure 4 Discharge/charge curves of (a) S/HCSF cathode and (b) S/HCSF@C-1 cathode at a current density of 100 mA/g. Rate capabilities of (c) S/HCSF cathode and (d) S/HCSF@C-1 cathode. (e) Cycling performances and CE of S/HCSF cathode and S/HCSF@C-1 cathode at a current density of 500 mA/g.

two obvious reaction plateaus were clearly observed in the discharge process of the as-synthesized sulfur/carbon cathodes. The first plateau at 2.4 V can be attributed to the redox reaction from solid elemental S_8 to liquid long-chain lithium polysulfides (Li_2S_x, $4 \leqslant x \leqslant 8$). The second plateau at 2.1 V corresponds to the deep redox reaction of liquid long-chain lithium polysulfides to give solid short-chain lithium polysulfides (Li_2S_2 and Li_2S). Such a discharge profile is typical for sulfur cathodes and agrees well with previous reports [32, 45]. Based on the discharge curves, the S/HCSF cathode was able to deliver 1,409 mAh/g (all of the capacity values in this work are calculated according to the mass of sulfur) in its first discharge process, which is slightly higher than the value of 1,347 mAh/g for S/HCSF@C-1. The initial capacities of the S/HCSF and S/HCSF@C-1 cathode are about 84% and 81% of the theoretical capacity of sulfur, respectively. The high initial discharge capacities indicate that the highly dispersed sulfur impregnated in the pore structures of HCSF and HCSF@C-1 affords efficient electron transfer to the sulfur mass and accessibility to the electrolyte, resulting in high electrochemical utilization of sulfur. It is well known that the inevitable dissolution of polysulfides into the electrolyte causes severe capacity loss of sulfur/ carbon cathodes. Similar to most sulfur/carbon cathodes, the discharge capacities of the S/HCSF and S/HCSF@C-1 cathode calculated from the second cycle decrease to 1,227 and 1,142 mAh/g, respectively. After 30 cycles, S/HCSF has a capacity of 928 mAh/g, corresponding to a capacity retention of 76% compared with the second cycle. Interestingly, S/HCSF@C-1 still has a high discharge capacity (1,042 mAh/g) after 30 cycles. Compared with the second cycle, the capacity retention of the S/HCSF@C-1 cathode is about 91%. Since the capacity contribution of the second plateau in the discharge curve corresponds to the conversion of polysulfides (Li_2S_{4-8}) into Li_2S/Li_2S_2, the loss of polysulfides in the electrode during cycling can be evaluated by calculating the capacity of the second plateau [32]. The capacities of the second plateau in the S/HCSF cathode for the 1st, 2nd, and 30th cycles are 910, 820, and 560 mAh/g, respectively. In comparison, the capacities of the second plateau in the S/HCSF@C-1 cathode for the 1st, 2nd, and 30th cycles are 870, 770, and 750 mAh/g, respectively. It should be pointed out that S/HCSF and S/HCSF@C-1 electrodes have similar sulfur contents of ~70 wt.% meaning that the results are directly comparable. The large and stable capacity contribution from the second plateau reveals that the obtained hollow-in-hollow structure not only offers efficient sulfur utilization but also reduces the loss of active component. Furthermore, the S/HCSF@-1 cathode exhibits a lower charge-transfer resistance than the S/HCSF cathode (Fig. S3, in the ESM), indicating the preferable electrochemical environment provided by the hollow-in-hollow structure results in better performance [13].

Compared with the S/HCSF cathode, the S/HCSF@C-1 cathode also showed favorable high-rate capability (Figs. 4(c) and 4(d)). The discharge capacities of the S/HCSF cathode stabilized around 1,144, 843, 752, 667, and 535 mAh/g when cycled at 100, 200, 500, 1,000, and 2,000 mA/g, respectively. When the current density was switched back to 100 mA/g, the discharge capacity of the S/HCS cathode was about 944 mAh/g, which is 82% of the initial discharge capacity (1,144 mAh/g) at the same rate. On the basis of these results, a capacity retention ratio of ~47% was obtained when the current density was increased from 100 mA/g to 2 A/g. With the higher specific surface area and pore volumes, the rate capability of the S/HCSF cathode is better than the previously reported S/DHCS cathode [34]. In comparison, the S/HCSF@C-1 cathode exhibited not only much higher capacity at the same discharge rate but also a better capacity retention ratio of ~58% (from 1,095 mAh/g at 100 mA/g to 690 mAh/g at 2 A/g). Importantly, a reversible capacity of 1,093 mAh/g was obtained when the current was reduced back to 100 mA/g, which is close to the initial capacity (1,095 mAh/g), indicating the good stability of the S/HCSF@C-1 cathode at various rates. To further investigate the cycling stability of the as-synthesized sulfur/carbon composites, the S/HCSF and S/HCSF@C-1 cathodes were tested for 100 cycles at a high rate of 500 mA/g. As shown in Fig. 4(e), the initial discharge capacities of the S/HCSF and S/HCSF@C-1 cathode were 1,240 and 1,232 mAh/g, respectively. After 100 cycles, the discharge capacity of the S/HCSF cathode decayed from 1,240 to 807 mAh/g. In comparison, a higher

discharge capacity of 942 mAh/g was still retained for the S/HCS@C-1 cathode. The detailed discharge capacities of the S/HCSF and S/HCSF@C-1 cathodes at a charge/discharge rate of 500 mA/g are summarized in Table S1 (in the ESM). At the same time, the Coulombic efficiency (CE) of the S/HCS@C-1 cathode was more than 99%. Obviously, these results also indicate that the loss of active component (i.e., the "shuttling effect") in the S/HCS@C-1 cathode was well-suppressed compared with the S/HCSF cathode.

The higher capacity and rate performance of S/HCSF@C-1 cathode can be attributed to its unique hollow-in-hollow structure, in which sulfur was confined in the inner HCSF core. As illustrated in Scheme 1, the active component in the S/HCSF cathode is in direct contact with the electrolyte. During the charge/discharge process, the soluble polysulfide intermediates can easily detach from the electrode and leach into the electrolyte, leading to decreased capacity. In comparison, the hollow carbon shell of S/HCSF@C-1 can efficiently encapsulate the polysulfide anions derived from inner S/HCSF core and prevent their diffusion into the electrolyte, which limits the "shuttling effect" [46].

It is worth noting that although the hollow carbon shell of S/HCSF@C-1 can be utilized as an efficient polysulfide entrapment for the inner S/HCSF cores, the polysulfide derived from the hollow carbon shell of S/HCSF@C-1 still suffers from an inevitable "shuttling effect". To further minimize the dissolution of the polysulfide intermediates, a direct and available strategy is to increase the capacity contribution by the inner S/HCSF core. Considering that the sulfur content in the inner HCSF core and the outer carbon shell of the HCSF@C are related to the structure parameter of carbon layers, maximizing the sulfur filled in the inner HCSF core of HCSF@C (i.e., HCSF@C with a thin carbon shell) is desirable in order to enhance the capacity performance. Since our hard-templating procedures are highly tailorable, HCSF@C-0.5 with a 15 nm hollow carbon shell was synthesized by simply decreasing the dosage of the RF precursor when forming the outer hollow carbon shells (Figs. 5(a) and 5(b)) [43, 44].

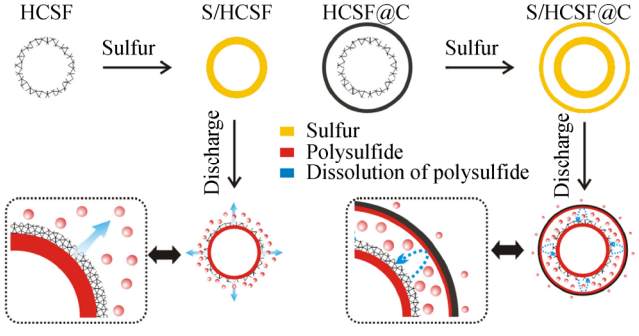

Scheme 1 Schematic illustration of the hollow-in-hollow structure for improving the performance of S/HCS cathodes.

After sulfur impregnation, the sulfur content in S/HCSF@C-0.5 composite was determined to be approximately 70.7 wt.% (Fig. S4, in the ESM). Compared with HCSF@C-1, most of sulfur was filled in the inner HCSF core of HCSF@C-0.5 (Fig. 5(c)). As expected, the capacity and rate performance of S/HCSF@C-0.5 cathode are substantially higher than the S/HCSF@C-1 cathode. When cycled at 100, 200, 500, 1,000, and 2,000 mA/g, the discharge capacities of the S/b-HCS-0.5 cathode were stabilized around 1,260, 1,102, 959, 909, and 801 mAh/g, respectively (Fig. 5(d)). The stability of the S/HCSF@C-0.5 cathode is evidenced by the recovery of a capacity of 1,120 mAh/g at 100 mA/g rate following charging at the high rate of 2 A/g. At charge/discharge rate of 500 mA/g, the S/HCSF@C-0.5 cathode still retained a high capacity of 991 mAh/g after 100 cycles (Fig. 5(e)). During cycling, the CE of the S/HCSF@C-0.5 cathode stabilized at around 99%. For comparison, HCSF@C-1.5 with 24 nm hollow carbon shell was also synthesized (Fig. S5, in the ESM). Not surprisingly, the rate performance and capacity of the S/HCSF@C-1.5 cathode with a sulfur content of 73.0 wt.% (Fig. S6, in the ESM) are only slightly higher than the corresponding values for the S/HCSF cathode (Fig. S7, in the ESM).

To further investigate the long-term cycling stability of the optimized sulfur/carbon cathode, the S/HCSF@C-0.5 cathode was tested for 300 cycles at a higher rate of 1 A/g (Fig. 5(f)). Without any initial conditioning cycles of activation and stabilization, the capacity of the S/HCSF@C-0.5 cathode still faded during the first two cycles. However, the S/HCSF@C-0.5 cathode can be stabilized and exhibited a reversible and comparable capacity after three cycles. As shown in Fig. 5(f), the S/HCSF@C-0.5 cathode exhibited a capacity of ~1,080 mAh/g at the third cycle and

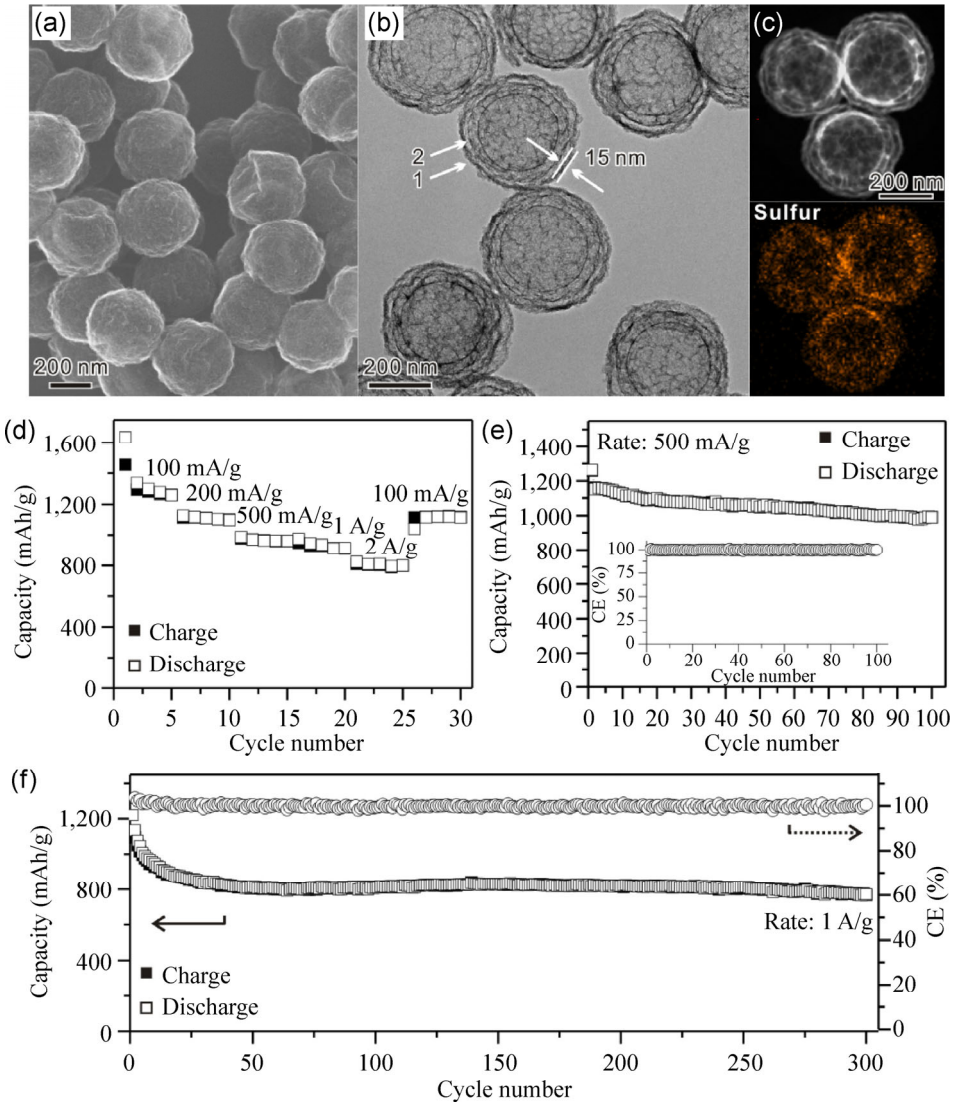

Figure 5 (a) SEM image and (b) TEM image of HCSF@C-0.5, (c) element mapping image of S/HCSF@C-0.5, (d) rate capabilities of the S/HCSF@C-0.5 cathode, (e) and (f) cycling performance of the S/HCSF@C-0.5 cathode at a current density of 500 mA/g (e) and 1 A/g (f), insert: the corresponding CE.

maintained a capacity of ~780 mAh/g after 300 cycles with capacity retention of 72.2% (a decay rate of 0.09% per cycle) and high CE up to 99%. After 300 cycles, the mass capacity, area capacity, and volumetric capacity of the overall electrode of S/HCSF@C-0.5 are 386 mAh/g, 0.37 mAh/cm^2, and 455 mAh/cm^3, respectively. More importantly, although undergoing a slightly faster capacity loss within the first 50 cycles (from 1,080 to 815 mAh/g), the S/HCSF@C-0.5 cathode retained a nearly constant capacity in the subsequent 250 cycles. From the 50th cycle to the 300th cycle, the capacity of the S/HCSF@C-0.5 cathode only decayed from 815 to 780 mAh/g, representing an extremely low decay rate of ~0.017% per cycle. Since the dissolution of the polysulfide intermediates derived from hollow carbon shell of S/HCSF@C was further suppressed, the performance of the S/HCSF@C-0.5 cathode is better than many previously reported sulfur/carbon cathodes and polymer or graphene coated sulfur/carbon cathodes (Table S2, in the ESM) [11, 46–48]. Our proposed strategy based on structure optimization can effectively improve the performance of the S/HCSF@C cathode, which makes HCSF@C promising material for application in lithium–sulfur batteries.

4 Conclusions

Hollow-in-hollow carbon spheres with hollow foam-like cores (i.e., HCSF@C) were successfully synthesized via a hard-templating method, using RF resin as a carbon precursor and solid SiO_2 spheres as the templates. Sulfur/carbon composites prepared from HCSF@C exhibit high sulfur content (70.7 wt.%). Compared with the S/HCSF cathode, the hollow-in-hollow structured S/HCSF@C cathode showed better capacity, rate capability, and cycling stability. The S/HCSF@C cathode retains a high capacity of 780 mAh/g after 300 cycles at a high charge/discharge rate of 1 A/g. The excellent performance of the S/HCSF@C cathode can be attributed to its unique hollow-in-hollow structure. The hollow carbon shell of S/HCSF@C can efficiently encapsulate the polysulfide derived from the inner S/HCSF core and significantly reduce the "shuttling effect". The hollow-in-hollow structured HCSF@C proposed in this work is a promising candidate for use in high-performance sulfur/carbon cathodes, and we believe that the synthesis of hollow-in-hollow structures can be extended to produce new carbon nanostructures with other inner carbon materials, such as graphene, porous carbon tubes, and metal–organic framework derived porous carbon for use as high-performance electrode materials [49, 50].

Acknowledgements

We thank the National Basic Research Program of China (Nos. 2011CB932403 and 2015CB932300) and the National Natural Science Foundation of China (Nos. 21301144, 21390390, 21131005, 21333008, and 21420102001) for financial support.

Electronic Supplementary Material: Supplementary material (TGA curve of S/HCSF@C-0.5, SEM images, TEM images, TGA curve, rate capabilities, and cycling performance of S/HCSF@C-1.5 cathode) is available in the online version of this article at http://dx.doi.org/10.1007/s12274-015-0773-3.

References

[1] Bruce, P. G.; Freunberger, S. A.; Hardwick, L. J.; Tarascon, J. M. Li-O_2 and Li-S batteries with high energy storage. *Nat. Mater.* **2012**, *11*, 19–29.

[2] Evers, S.; Nazar, L. F. New approaches for high energy density lithium-sulfur battery cathodes. *Acc. Chem. Res.* **2013**, *46*, 1135–1143.

[3] Manthiram, A.; Fu, Y. Z.; Su, Y. S. Challenges and prospects of lithium-sulfur batteries. *Acc. Chem. Res.* **2013**, *46*, 1125–1134.

[4] Yin, Y. X.; Xin, S.; Guo, Y. G.; Wan, L. J. Lithium-sulfur batteries: Electrochemistry, materials, and prospects. *Angew. Chem. Int. Ed.* **2013**, *52*, 13186–13200.

[5] Yang, Y.; Zheng, G. Y.; Cui, Y. Nanostructured sulfur cathodes. *Chem. Soc. Rev.* **2013**, *42*, 3018–3032.

[6] Armstrong, M. J.; O'Dwyer, C.; Macklin, W. J.; Holmes, J. D. Evaluating the performance of nanostructured materials as lithium-ion battery electrodes. *Nano Res.* **2014**, *7*, 1–62.

[7] Ji, X. L.; Lee, K. T.; Nazar, L. F. A highly ordered nanostructured carbon-sulphur cathode for lithium-sulphur batteries. *Nat. Mater.* **2009**, *8*, 500–506.

[8] Ji, L. W.; Rao, M. M.; Zheng, H. M.; Zhang, L.; Li, Y. C.; Duan, W. H.; Guo, J. H.; Cairns, E. J.; Zhang, Y. G. Graphene oxide as a sulfur immobilizer in high performance lithium/sulfur cells. *J. Am. Chem. Soc.* **2011**, *133*, 18522–18525.

[9] Wang, Z. Y.; Dong, Y. F.; Li, H. J.; Zhao, Z. B.; Wu, H. B.; Hao, C.; Liu, S. H.; Qiu, J. S.; Lou, X. W. Enhancing lithium-sulphur battery performance by strongly binding the discharge products on amino-functionalized reduced graphene oxide. *Nat. Commun.* **2014**, *5*, 5002.

[10] Xiao, L. F.; Cao, Y. L.; Xiao, J.; Schwenzer, B.; Engelhard, M. H.; Saraf, L. V.; Nie, Z. M.; Exarhos, G. J.; Liu, J. A soft approach to encapsulate sulfur: Polyaniline nanotubes for lithium-sulfur batteries with long cycle life. *Adv. Mater.* **2012**, *24*, 1176–1181.

[11] Yang, Y.; Yu, G. H.; Cha, J. J.; Wu, H.; Vosgueritchian, M.; Yao, Y.; Bao, Z. N.; Cui, Y. Improving the performance of lithium-sulfur batteries by conductive polymer coating. *ACS Nano* **2011**, *5*, 9187–9193.

[12] Li, W. Y.; Zhang, Q. F.; Zheng, G.; Seh, Z. W.; Yao, H. B.; Cui, Y. Understanding the role of different conductive polymers in improving the nanostructured sulfur cathode performance. *Nano Lett.* **2013**, *13*, 5534–5540.

[13] Qiu, Y. C.; Li, W. F.; Li, G. Z.; Hou, Y.; Zhou, L. S.; Li, H. F.; Liu, M. N.; Ye, F. M.; Yang, X. W.; Zhang, Y. G. Polyaniline-modified cetyltrimethylammonium bromide–graphene oxide–sulfur nanocomposites with enhanced performance for lithium-sulfur batteries. *Nano Res.* **2014**, *7*, 1355–1363.

[14] Seh, Z. W.; Li, W.; Cha, J. J.; Zheng, G. Y.; Yang, Y.; McDowell, M. T.; Hsu, P. C.; Cui, Y. Sulphur-TiO_2 yolk-shell nanoarchitecture with internal void space for long-cycle lithium-sulphur batteries. *Nat. Commun.* **2013**, *4*, 1331.

[15] Zhou, W. D.; Yu, Y. C.; Chen, H.; DiSalvo, F. J.; Abruna, H. D. Yolk-shell structure of polyaniline-coated sulfur for lithium-sulfur batteries. *J. Am. Chem. Soc.* **2013**, *135*, 16736–16743.

[16] Su, Y. S.; Manthiram, A. Lithium-sulphur batteries with a microporous carbon paper as a bifunctional interlayer. *Nat. Commun.* **2012**, *3*, 1166.

[17] Zhang, S. S. Role of $LiNO_3$ in rechargeable lithium/sulfur battery. *Electrochim. Acta* **2012**, *70*, 344–348.

[18] Schuster, J.; He, G.; Mandlmeier, B.; Yim, T.; Lee, K. T.; Bein, T.; Nazar, L. F. Spherical ordered mesoporous carbon nanoparticles with high porosity for lithium-sulfur batteries. *Angew. Chem. Int. Ed.* **2012**, *51*, 3591–3595.

[19] Li, Z.; Yuan, L. X.; Yi, Z. Q.; Sun, Y. M.; Liu, Y.; Jiang, Y.; Shen, Y.; Xin, Y.; Zhang, Z. L.; Huang, Y. H. Insight into the electrode mechanism in lithium-sulfur batteries with ordered microporous carbon confined sulfur as the cathode. *Adv. Energy Mater.* **2014**, *4*, 1301473.

[20] Wu, H. B.; Wei, S. Y.; Zhang, L.; Xu, R.; Hng, H. H.; Lou, X. W. Embedding sulfur in MOF-derived microporous carbon polyhedrons for lithium-sulfur batteries. *Chem.—Eur. J.* **2013**, *19*, 10804–10808.

[21] Jung, D. S.; Hwang, T. H.; Lee, J. H.; Koo, H. Y.; Shakoor, R. A.; Kahraman, R.; Jo, Y. N.; Park, M. S.; Choi, J. W. Hierarchical porous carbon by ultrasonic spray pyrolysis yields stable cycling in lithium-sulfur battery. *Nano Lett.* **2014**, *14*, 4418–4425.

[22] Li, Z.; Jiang, Y.; Yuan, L. X.; Yi, Z. Q.; Wu, C.; Liu, Y.; Strasser, P.; Huang, Y. H. A highly ordered meso@microporous carbon-supported sulfur@smaller sulfur core-shell structured cathode for Li-S batteries. *ACS Nano* **2014**, *8*, 9295–9303.

[23] Guo, J. Z.; Xu, Y. H.; Wang, C. S. Sulfur-impregnated disordered carbon nanotubes cathode for lithium-sulfur batteries. *Nano Lett.* **2011**, *11*, 4288–4294.

[24] Zheng, G. Y.; Yang, Y.; Cha, J. J.; Hong, S. S.; Cui, Y. Hollow carbon nanofiber-encapsulated sulfur cathodes for high specific capacity rechargeable lithium batteries. *Nano Lett.* **2011**, *11*, 4462–4467.

[25] Zhou, G. M.; Yin, L. C.; Wang, D. W.; Li, L.; Pei, S. F.; Gentle, I. R.; Li, F.; Cheng, H. M. Fibrous hybrid of graphene and sulfur nanocrystals for high-performance lithium-sulfur batteries. *ACS Nano* **2013**, *7*, 5367–5375.

[26] Yang, X.; Zhang, L.; Zhang, F.; Huang, Y.; Chen, Y. S. Sulfur-infiltrated graphene-based layered porous carbon cathodes for high-performance lithium-sulfur batteries. *ACS Nano* **2014**, *8*, 5208–5215.

[27] Zhou, G. M.; Wang, D. W.; Li, F.; Hou, P. X.; Yin, L. C.; Liu, C.; Lu, G. Q.; Gentle, I. R.; Cheng, H. M. A flexible nanostructured sulphur-carbon nanotube cathode with high rate performance for Li-S batteries. *Energy Environ. Sci.* **2012**, *5*, 8901–8906.

[28] Yao, H. B.; Zheng, G. Y.; Li, W. Y.; McDowell, M. T.; Seh, Z. W.; Liu, N. A.; Lu, Z. D.; Cui, Y. Crab shells as sustainable templates from nature for nanostructured battery electrodes. *Nano Lett.* **2013**, *13*, 3385–3390.

[29] Chen, X. A.; Xiao, Z. B.; Ning, X. T.; Liu, Z.; Yang, Z.; Zou, C.; Wang, S.; Chen, X. H.; Chen, Y.; Huang, S. M. Sulfur-impregnated, sandwich-type, hybrid carbon nanosheets with hierarchical porous structure for high-performance lithium-sulfur batteries. *Adv. Energy Mater.* **2014**, *4*, 1301988.

[30] Li, Y. Y.; Li, Z. S.; Zhang, Q. W.; Shen, P. K. Sulfur-infiltrated three-dimensional graphene-like material with hierarchical pores for highly stable lithium-sulfur batteries. *J. Mater. Chem. A* **2014**, *2*, 4528–4533.

[31] Xin, S.; Gu, L.; Zhao, N. H.; Yin, Y. X.; Zhou, L. J.; Guo, Y. G.; Wan, L. J. Smaller sulfur molecules promise better lithium-sulfur batteries. *J. Am. Chem. Soc.* **2012**, *134*, 18510–18513.

[32] Sun, L.; Li, M. Y.; Jiang, Y.; Kong, W. B.; Jiang, K. L.; Wang, J. P.; Fan, S. S. Sulfur nanocrystals confined in carbon nanotube network as a binder-free electrode for high-performance lithium sulfur batteries. *Nano Lett.* **2014**, *14*, 4044–4049.

[33] Jayaprakash, N.; Shen, J.; Moganty, S. S.; Corona, A.; Archer, L. A. Porous hollow carbon@sulfur composites for high-power lithium-sulfur batteries. *Angew. Chem. Int. Ed.* **2011**, *50*, 5904–5908.

[34] Zhang, C. F.; Wu, H. B.; Yuan, C. Z.; Guo, Z. P.; Lou, X. W. Confining sulfur in double-shelled hollow carbon spheres for lithium-sulfur batteries. *Angew. Chem. Int. Ed.* **2012**, *51* 9592 –9595.

[35] Zhang, K.; Zhao, Q.; Tao, Z. L.; Chen, J. Composite of sulfur impregnated in porous hollow carbon spheres as the cathode of Li-S batteries with high performance. *Nano Res.* **2013**, *6*, 38–46.

[36] He, G.; Evers, S.; Liang, X.; Cuisinier, M.; Garsuch, A.; Nazar, L. F. Tailoring porosity in carbon nanospheres for lithium-sulfur battery cathodes. *ACS Nano* **2013**, *7*, 10920–10930.

[37] Zhao, M. Q.; Zhang, Q.; Huang, J. Q.; Tian, G. L.; Nie, J. Q.; Peng, H. J.; Wei, F. Unstacked double-layer templated graphene for high-rate lithium-sulphur batteries. *Nat. Commun.* **2014**, *5*, 3410.

[38] Zhou, W. D.; Xiao, X. C.; Cai, M.; Yang, L. Polydopamine-coated, nitrogen-doped, hollow carbon-sulfur double-layered core-shell structure for improving lithium-sulfur batteries. *Nano Lett.* **2014**, *14*, 5250–5256.

[39] Liu, J.; Qiao, S. Z.; Chen, J. S.; Lou, X. W.; Xing, X. R.; Lu, G. Q. Yolk/shell nanoparticles: New platforms for

nanoreactors, drug delivery and lithium-ion batteries. *Chem. Commun.* **2011**, *47*, 12578–12591.

[40] Fang, X. L.; Zhao, X. J.; Fang, W. J.; Chen, C.; Zheng, N. F. Self-templating synthesis of hollow mesoporous silica and their applications in catalysis and drug delivery. *Nanoscale* **2013**, *5*, 2205–2218.

[41] Wang, J. Y.; Yang, N. L.; Tang, H. J.; Dong, Z. H.; Jin, Q.; Yang, M.; Kisailus, D.; Zhao, H. J.; Tang, Z. Y.; Wang, D. Accurate control of multishelled Co_3O_4 hollow microspheres as high-performance anode materials in lithium-ion batteries. *Angew. Chem. Int. Ed.* **2013**, *52*, 6417–6420.

[42] Zhang, G. Q.; Lou, X. W. General synthesis of multi-shelled mixed metal oxide hollow spheres with superior lithium storage properties. *Angew. Chem. Int. Ed.* **2014**, *53*, 9041–9044.

[43] Fang, X. L.; Liu, S. J.; Zang, J.; Xu, C. F.; Zheng, M. S.; Dong, Q. F.; Sun, D. H.; Zheng, N. F. Precisely controlled resorcinol-formaldehyde resin coating for fabricating core-shell, hollow, and yolk-shell carbon nanostructures. *Nanoscale* **2013**, *5*, 6908–6916.

[44] Fang, X. L.; Zang, J.; Wang, X. L.; Zheng, M. S.; Zheng, N. F. A multiple coating route to hollow carbon spheres with foam-like shells and their applications in supercapacitor and confined catalysis. *J. Mater. Chem. A* **2014**, *2*, 6191–6197.

[45] Zhao, Y.; Wu, W. L.; Li, J. X.; Xu, Z. C.; Guan, L. H. Encapsulating MWNTs into hollow porous carbon nanotubes: A tube-in-tube carbon nanostructure for high-performance lithium-sulfur batteries. *Adv. Mater.* **2014**, *26*, 5113–5118.

[46] Lu, S. T.; Cheng, Y. W.; Wu, X. H.; Liu, J. Significantly improved long-cycle stability in high-rate Li-S batteries enabled by coaxial graphene wrapping over sulfur-coated carbon nanofibers. *Nano Lett.* **2013**, *13*, 2485–2489.

[47] Wang, L.; Wang, D.; Zhang, F. X.; Jin, J. Interface chemistry guided long-cycle-life Li-S battery. *Nano Lett.* **2013**, *13*, 4206–4211.

[48] Wang, H. L.; Yang, Y. Y.; Liang, Y.; Robinson, J. T.; Li, Y. G.; Jackson, A.; Cui, Y.; Dai, H. J. Graphene-wrapped sulfur particles as a rechargeable lithium-sulfur battery cathode material with high capacity and cycling stability. *Nano Lett.* **2011**, *11*, 2644–2647.

[49] Zheng, J. M.; Tian, J.; Wu, D. X.; Gu, M.; Xu, W.; Wang, C. M.; Gao, F.; Engelhard, M. H.; Zhang, J. G.; Liu, J. et al. Lewis acid-base interactions between polysulfides and metal organic framework in lithium sulfur batteries. *Nano Lett.* **2014**, *14*, 2345–2352.

[50] Zhou, J. W.; Li, R.; Fan, X. X.; Chen, Y. F.; Han, R. D.; Li, W.; Zheng, J.;Wang, B.; Li, X. G. Rational design of a metal-organic framework host for sulfur storage in fast, long-cycle Li-S batteries. *Energy Environ. Sci.* **2014**, *7*, 2715–2724.